



THE UNIVERSITY *of* EDINBURGH

Edinburgh Research Explorer

MTSS1/Src family kinase Dysregulation Underlies Multiple Inherited Ataxias

Citation for published version:

Brown, AS, Meera, P, Altindag, B, Chopra, R, Perkins, E, Paul, S, Scoles, DR, Tarapore, E, Magri, J, Huang, H, Jackson, M, Shakkottai, VG, Otis, TS, Pulst, SM, Atwood, SX & Oro, AE 2018, 'MTSS1/Src family kinase Dysregulation Underlies Multiple Inherited Ataxias', *Proceedings of the National Academy of Sciences (PNAS)*. <https://doi.org/10.1073/pnas.1816177115>

Digital Object Identifier (DOI):

[10.1073/pnas.1816177115](https://doi.org/10.1073/pnas.1816177115)

Link:

[Link to publication record in Edinburgh Research Explorer](#)

Document Version:

Peer reviewed version

Published In:

Proceedings of the National Academy of Sciences (PNAS)

General rights

Copyright for the publications made accessible via the Edinburgh Research Explorer is retained by the author(s) and / or other copyright owners and it is a condition of accessing these publications that users recognise and abide by the legal requirements associated with these rights.

Take down policy

The University of Edinburgh has made every reasonable effort to ensure that Edinburgh Research Explorer content complies with UK legislation. If you believe that the public display of this file breaches copyright please contact openaccess@ed.ac.uk providing details, and we will remove access to the work immediately and investigate your claim.



BIOLOGICAL SCIENCES: Neuroscience, cell biology

MTSS1/Src family kinase Dysregulation Underlies Multiple Inherited Ataxias

Alexander S. Brown¹, Pratap Meera², Banu Altindag¹, Ravi Chopra³, Emma Perkins⁴,
Sharan Paul⁵, Daniel R. Scoles⁵, Eric Tarapore⁷, Jessica Magri¹, Haoran Huang³, Mandy
Jackson⁴, Vikram G. Shakkottai³, Thomas S. Otis⁶, Stefan M. Pulst⁵, Scott X. Atwood^{1,7,8},
Anthony E. Oro^{1,8}

Affiliations: ¹Program in Epithelial Biology, Stanford University School of Medicine
Stanford, CA 94305, ²Department of Neurobiology, University of California, Los Angeles,
Los Angeles, CA, ³Department of Neurology, University of Michigan, Ann Arbor, MI,
⁴Centre for Discovery Brain Sciences, University of Edinburgh, Edinburgh, United
Kingdom, ⁵Department of Neurology, University of Utah Medical Center, Salt Lake City,
UT, ⁶Sainsbury Wellcome Centre for Neural Circuits and Behavior, University College
London, London, United Kingdom, ⁷Department of Developmental and Cell Biology,
University of California, Irvine,

Address correspondence to:

Anthony E. Oro oro@stanford.edu (Lead Contact), Alexander Brown
sale@stanford.edu, or Scott X Atwood satwood@uci.edu

Abstract (153/250 words)

The genetically heterogeneous Spinocerebellar ataxias (SCAs) are caused by Purkinje neuron dysfunction and degeneration, but their underlying pathological mechanisms remain elusive. The Src family of non-receptor tyrosine kinases (SFK) are essential for nervous system homeostasis and are increasingly implicated in degenerative disease. Here we reveal that the SFK suppressor Missing-in-Metastasis (MTSS1) is an ataxia locus that links multiple SCAs. MTSS1 loss results in increased SFK activity, reduced Purkinje neuron arborization, and low basal firing rates, followed by cell death. Surprisingly, mouse models for SCA1, SCA2, and SCA5 show elevated SFK activity, with SCA1 and SCA2 displaying dramatically reduced MTSS1 protein levels through reduced gene expression and protein translation, respectively. Treatment of each SCA model with a clinically-approved Src inhibitor corrects Purkinje basal firing, and delays ataxia progression in MTSS1 mutants. Our results identify a common SCA therapeutic target and demonstrate a key role for MTSS1/SFK in Purkinje neuron survival and ataxia progression.

Keywords: Neurodegeneration, Src Kinase, MTSS1, Bar Domain Proteins, Actin Cytoskeleton, Spinocerebellar ataxia, SCA1, SCA2, Src kinase Inhibitor, RNA binding protein, Translation

Significance Statement (120/120)

The Src family of non-receptor tyrosine kinases (SFK) are essential for nervous system function, and may contribute to neurodegeneration. Spinocerebellar ataxias (SCAs) are neurodegenerative diseases where Purkinje neurons fire irregularly and degenerate leading to motor problems. We show that the SFK suppressor Missing-in-Metastasis (MTSS1) is an ataxia gene that links multiple SCAs. MTSS1 loss results in increased SFK activity, degenerating Purkinje neurons with low firing rates, and cell death. Surprisingly, mouse models for three different SCAs show elevated SFK activity, with SCA1 and SCA2 models displaying dramatically reduced MTSS1 protein levels. Treatment of each SCA model with SFK inhibitor corrects Purkinje basal firing, and delays ataxia progression in MTSS1 mutants. Our results identify a common link among disparate neurodegenerative diseases.

75 \body

76 **Introduction**

77 Neurons are non-dividing cells that depend on homeostatic regulation of protein,
78 RNA, and metabolite turnover to permit dynamic synaptic connections that allow
79 adaptation to changing environments. Loss of such mechanisms result in one of several
80 hundred neurodegenerative disorders. Over 40 loci form the genetic basis for human
81 Spinocerebellar Ataxia (SCA), a progressive motor disorder characterized by cerebellar
82 atrophy and pervasive Purkinje neuron degeneration where patients experience poor
83 coordination and balance, hand-eye coordination, dysarthria, and abnormal saccades.

84 One common phenotype prominent in multiple SCA animal models is the altered
85 Purkinje neuron firing rates that precede motor impairment and cell death (1-3), with
86 restoration of the normal firing rates reducing Purkinje neuron death and improving
87 motor function (4, 5). Defects in many cell functions lead to SCA including effectors of
88 transcription (6), translation (7), proteostasis (8, 9), calcium flux (10, 11), and
89 cytoskeletal/membrane interactions (12, 13). An open question remains how the many
90 SCA genes interact to control firing rates and cell survival, with a common target
91 emerging as an ideal treatment for the genetically diverse etiologies.

92 One such therapeutic target is the class of Src family of non-receptor tyrosine kinases
93 (SFKs). Several SFKs are expressed in the nervous system and have partially
94 overlapping functions. While single mutants for *Src* or *Yes* kinase have no overt
95 neuronal phenotype (14, 15), *Fyn* loss of function leads to increased *Src* activity and
96 hippocampal learning and memory deficits (16, 17). Moreover, *Fyn;Src* double mutants
97 rarely survive past birth and have severely disorganized cortical and cerebellar layers
98 (15, 18). SFKs are post-translationally regulated through activating and inhibitory
99 phosphorylation marks deposited by inhibitory kinases and removed by receptor tyrosine
100 phosphatases in a context dependent manner (19, 20). SFK activation occurs rapidly in
101 response to extracellular signals and in response to a variety of cellular stresses ranging
102 from osmotic pressure (21) to tetanic stimulation (22). Additionally, SFKs are
103 inappropriately active in disease states including Amyotrophic lateral sclerosis (23),
104 Alzheimer disease (24), and Duchenne muscular dystrophy (25).

105 Missing-in-Metastasis (MTSS1) is one of the defining members of the I-BAR
106 family of negative membrane curvature sensing proteins first identified as being deleted
107 in metastatic bladder cancer (26). Although MTSS1 biochemically interacts with
108 membranes and regulates the actin cytoskeleton (27), genetic studies reveal that
109 MTSS1 functions in an evolutionarily conserved signaling cassette to antagonize Src

kinase activity (28, 29). Disruption of the MTSS1/Src regulatory cassette results in endocytosis and polarization abnormalities demonstrated by defects in primary cilia dependent hedgehog signaling, and hair follicle epithelial migration (28). In tissues requiring MTSS1 function, levels of active MTSS1 are critical, as loss (26) or gain (30) of MTSS1 has been associated with metastasis and invasion. Regardless of the particular phenotype, an evolutionarily conserved property of MTSS1 mutants is that loss of MTSS1 function can be reversed through the removal or inhibition of Src kinases. This property was first demonstrated through double mutant analysis in the fly ovary, and subsequently in mammalian tissue culture using Src family kinase inhibitors (28, 29). The availability of FDA-approved Src kinase inhibitors has led to the investigation of clinically relevant MTSS1 phenotypes with the hope of using SFK inhibitors to ameliorate them.

Although SFKs have been shown to regulate multiple classes of neurotransmitter receptors (31) they also function to control basic cytoskeletal components. Src regulates local actin polymerization (32) and endocytic receptor internalization (32-35). The actin cytoskeleton plays a critical role in cell signaling, proliferation, motility, and survival. Local, rather than global, actin dynamics control homeostatic synaptic signaling, and abnormalities in actin regulation underlie a diversity of psychiatric and neuronal diseases including Amyotrophic lateral sclerosis (36), Schizophrenia, Autism Spectrum Disorders (37), and motor dysfunction such as spinocerebellar ataxia (SCA) (38). A major challenge remains to understand how actin cytoskeletal regulation controls synaptic function and to develop improved therapeutics for these common and poorly-treated diseases.

Here we reveal that actin regulator and SFK antagonist *Mtss1* is an ataxia locus regulated by multiple SCA alleles that subsequently result in SFK hyper-activation. We show that clinically-available Src inhibitors correct Purkinje neuron firing rates and delay ataxia progression, demonstrating a novel and druggable role for the evolutionarily conserved MTSS1/SFK network in Purkinje neuron survival and ataxia progression.

Results

Mtss1 null mice display a progressive ataxia

Mtss1 functions in many tissues, and previous mutant alleles disrupting 5' exons resulted in mild lymphagenesis (39), progressive kidney disease (40), mild neurological phenotypes (41) and cerebellar dysfunction(42). However, *Mtss1* has

several possible internal promoters (43), and multiple splice variants with differing sub-cellular localization (44), and existing mutant lines display MTSS1 proteins (40, 45). As an alternative approach we generated a conditional mutant allele targeting the endophilin/Src interacting domain located in the final exon (*MIM^{EX15}*, **Fig 1A**) (28, 29). Germline deletion with HPRT-cre resulted in the loss of MTSS1 protein as detected by an antibody specific to the N-terminal IMD domain (30) (**Fig 1B**).

To our surprise, homozygous *MIM^{EX15}* mutants appear normal for cilia dependent processes with no observed instances of holoprosencephaly or polydactyly after multiple generations. Additionally, *MIM^{EX15}* mutant males are fertile. Instead, *MIM^{EX15}* mutants display a striking and progressive ataxia. To better understand the nature of *MIM^{EX15}* ataxia, we characterized *MIM^{EX15}* mutants using an open field test to evaluate gross motor control. *MIM^{EX15}* mutants had reduced velocity (**Fig 1C**) and rearing behavior (**Fig 1D**), consistent with overall movement defects. To uncouple possible motor and behavioral abnormalities we evaluated *MIM^{EX15}* mutants with rotarod assay and observed coordination abnormalities in as early as 4 weeks of age (**Fig 1E**). Many spinocerebellar ataxias display progressive neurologic phenotypes. To determine whether *MIM^{EX15}* animals showed progressive deterioration we employed a composite test measuring gait, grip strength and balance (46). We found *MIM^{EX15}* animals performed consistently worse than controls, with severity increasing with age (**Fig 1F**). *MIM^{EX15}* heterozygous animals displayed 75% of normal protein levels (**SI Appendix, Fig S1C**), giving no overt phenotype.

Reduced *Mtss1* levels are associated with a variety of cellular phenotypes including reduced presentation of receptors on the cell membrane (47), and altered Purkinje neuron morphology (41, 44). To determine the basis of the motor abnormalities and to distinguish among these possibilities we performed histological analysis. At 4 weeks, *MIM^{EX15}* mice are ataxic, yet their cerebella appeared grossly normal with intact granule, Purkinje neuron, and molecular layers. However, *MIM^{EX15}* mutants displayed a progressive loss of Purkinje neurons in all cerebellar lobes readily seen by 8 weeks of age (**Fig S1A**). Whereas wild type cerebella contain approximately 8 Purkinje neurons in a 250 μ m linear distance, 8-week old mice retained only 25% of wild type, and 36 week *MIM^{EX15}* mutants contained only 5% of the total number of Purkinje neurons (**Fig 1G**).

While ataxia genes can act in many cell types to regulate Purkinje cell function, MTSS1 is highly expressed in Purkinje cells, suggesting it is required in these cells for normal Purkinje cell function and survival. To confirm the Purkinje neuron defects seen

in *MIM^{EX15}* animals are due to a cell autonomous requirement for *Mtss1*, we conditionally inactivated *Mtss1* using the Purkinje neuron specific L7-Cre (*MIM^{cko}*) then compared Purkinje neuron morphology and loss to the global *MIM^{EX15}* mutant. *MIM^{cko}* Purkinje neurons were mosaic for MTSS1 expression likely due to inefficient LoxP recombination as the MTSS1 antibody showed high specificity (**SI Appendix Fig S1B**). At 20 weeks *MIM^{cko}* had a significant reduction in Purkinje neurons. In remaining Purkinje neurons, those lacking MTSS1 protein displayed thickened dendritic branches and reduced arbor volume, while neighboring Purkinje neurons with MTSS1 protein appeared normal (**Fig 1H**). We conclude that *Mtss1* acts cell autonomously in Purkinje neurons to maintain dendritic structure, with loss of MTSS1 resulting in abnormalities and eventual cell death.

Mtss1 mutant neurons display limited autophagic markers

An emergent mechanism of cell loss during neurodegeneration is aberrant macroautophagy. Autophagy is essential for Purkinje neuron survival, as loss of autophagy (48, 49) results in cell death. Increased levels of early autophagy markers have been described in multiple neurodegenerative diseases including Huntington's disease (50), Alzheimer disease (51), and SCA3 (52). *MIM^{EX15}* mutants partially fit this pattern of disease as we observed some signs of autophagy. As early as 4 weeks, we observed increased Complex V/ATP synthase staining indicative of fused mitochondria as well as dramatically reduced staining for the Golgi body marker Giantin (**Fig 2A**). We also observed increased transcript abundance for the early autophagy effector *VMP1* (53). By 8 weeks of age we could detect increased LC3-II species (**Fig 2B, SI Appendix S2A**), and electron microscopy revealed several autophagy related morphologies including swollen mitochondria, fragmented golgi bodies, lamellar bodies and double membrane autophagic vacuoles (**Fig S2C**). Interestingly, we were unable to detect increased *Sqstrm1* (p62) transcript or protein levels in *MIM^{EX15}*, an autophagocytic adapter protein associated with protein aggregation neurodegenerative disease (54) (**Fig S2B**). *MIM^{EX15}* animals displayed increased neuroinflammation shown by increased Aif1 transcript levels (**Fig 2D**), a readout of microglial infiltration. *MIM^{EX15}* animals also show increased GFAP positive glial infiltration (**Fig 2E, 2F, SI Appendix S1A**) consistent with reactive astroglyosis. Consistent with signs of autophagocytic cell death and neuroinflammation, we failed to see increased DNA breaks in *MIM^{EX15}* Purkinje neurons with TUNEL stain (**Fig 2G**).

Mtss1 prevents SFK dependent Purkinje neuron firing defects and ataxia

To characterize cellular changes associated with the ataxia present in 4-week old *MIM^{EX15}* mice, we examined the dendritic tree of individual biocytin injected Purkinje neurons (**Fig 3A**). Purkinje neuron dendritic arbor collapse has been observed in several SCA models including SCA1 (2), SCA5 (3), while many other models have shown thinned molecular layer including SCA2(1), SCA3 (55), that likely reflects reduced Purkinje dendritic volume. Similarly, *MIM^{EX15}* mutants showed a 60% reduction in the expansiveness of the dendritic tree (**Fig 3B**) and a significant decrease in the number of dendritic spines (**Fig 3C**), although no significant difference was detected in spine length (**Fig 3D**) or width (**Fig 3E**).

In dermal fibroblasts and *Drosophila* border cells MTSS1 functions to locally prevent ectopic Src kinase activity and *Mtss1* mutant phenotypes can be rescued by genetically removing Src kinase (28, 29). To determine if *Mtss1* acts similarly in Purkinje neurons we evaluated SFK activity levels in cerebellar lysates from *MIM^{EX15}* mutants and found elevated levels of SFK^{Y416} (**Fig 3F**) indicative of increased SFK activity. Previous work has shown strong functional interactions between SFK and metabotropic glutamate receptor type I (mGluR1) neurotransmission at parallel fiber synapse (56). To investigate whether MTSS1/SFK modulation of mGluR1 signaling forms the basis of the ataxia, we performed electrophysiological analysis of Purkinje neurons in cerebellar slices from *MIM^{EX15}* mice. We evaluated Purkinje neuron response to parallel fiber stimulation using calcium imaging. We found *MIM^{EX15}* mutant Purkinje neurons responded with a comparable increase of calcium dependent fluorescence to controls, while adding the mGluR1 antagonist CPCCOEt abolished these responses (**Fig 3G**). These data support MTSS1 acting post-synaptically to control Purkinje cell function.

Purkinje neurons maintain a cell autonomous tonic firing rate that is essential for their function (57, 58). Since *MIM^{EX15}* Purkinje neurons responded normally to parallel fiber stimulation suggesting normal synaptic transmission, we assayed basal firing rate. Purkinje neuron tonic firing rate is highly sensitive to temperature and may vary slightly between investigators (59). In our assays, wild type cells had a mean firing rate of 43±2Hz (n=2 animals, 62 cells), while 4-week old *MIM^{EX15}* mutants exhibited a 12±1Hz mean rate (n=2 animals, 55 cells) (**Figs 3H, 3I**). Previous studies of SCA mouse models demonstrated reduced tonic firing is a basis for ataxia (1, 3, 5). Since basal firing is reduced at an age when *MIM^{EX15}* mice possess a normal number of Purkinje neurons, our results suggest neuron malfunction rather than loss underlies the initial ataxia phenotype.

MTSS1/Src double mutants rescue MTSS1 phenotypes in *Drosophila* and vertebrate cell culture. To test the hypothesis that reducing SFK activity would ameliorate the *MIM*^{EX15} ataxia phenotype, we added the FDA-approved SFK inhibitor dasatinib to cerebellar slice preparations and measured basal firing rate, using a concentration approximately 2-fold over *in vivo* IC50 (200nM, **Fig 3H, 3I**). Dasatinib significantly increased the *MIM*^{EX15} basal firing rate from baseline to 29±1Hz (n=2 animals, 62 cells). We also observed that dasatinib slightly reduced the wild type basal firing rate to 35±1Hz (n=2 animals, 79 cells). Time course experiments showed the increase in basal firing rate occurred over 5 hours (**SI Appendix Fig S3**), consistent with a low concentration, high affinity mechanism of action. Direct modulation of ion channel or mGluR1 activity raises basal firing within minutes (4, 60), suggesting that dasatinib works through a distinct mechanism. To determine whether SFK inhibition ameliorates ataxia *in vivo* we administered dasatinib directly to the cerebellum via minipumps to overcome poor CNS bioavailability (61). Over 4 weeks, dasatinib treated *MIM*^{EX15} mice were protected from disease progression while untreated mice showed progressively worsening rotarod performance (**Fig 3J**) (n=2 drug, 3 control). These results demonstrate that Src family kinases act downstream of MTSS1 and that SFK inhibitors rescue *Mtss1*-dependent basal firing rate defects to slow disease progression.

***Mtss1* is a translation target of ATXN2**

The slow basal firing and ataxia preceding cell death seen in the *MIM*^{EX15} mutants resembles that seen in other SCA models such as SCA1, SCA2, and SCA5, prompting us to investigate whether MTSS1/SFK dysregulation occurs in other ataxias. SCA2 is caused by an expansion in the polyglutamine (polyQ) tract of the RNA binding protein ATAXIN-2 (ATXN2) to more than 34 repeats (62). The exact molecular defects that drive SCA2 pathogenesis remain unclear, as loss of function mice do not recapitulate the SCA2 phenotype (63), while intermediate expansion alleles are associated with increased risk for frontotemporal dementia (64). *Atxn2* has an ancestral role in translation control (7, 65), which may be altered with the SCA2 mutation, but the exact targets have yet to be described.

MTSS1 protein abundance is heavily regulated by metastasis-associated miRs which bind to the *Mtss1* 3' untranslated region and reduce steady-state MTSS1 protein levels (66-70). To determine whether MTSS1 protein accumulation is sensitive to *Atxn2* we examined the *ATXN2*^{Q127} mouse model of SCA2 (1). We found MTSS1 abundance

was progressively reduced by 90% at 24 weeks, a level far greater than the 50% reduction in Purkinje neuron marker Calbindin (**Fig 4A upper band, SI Appendix Fig S4**). Cerebellar SFK activity was increased nearly 8-fold in *ATXN2*^{Q127} animals compared to wild type littermates (**Fig 4B**).

We sought to determine whether the age-dependent reduction in Purkinje neuron basal firing frequency seen in *ATXN2*^{Q127} mice is due to elevated SFK activity. Remarkably, addition of dasatinib to *ATXN2*^{Q127} cerebellar slices restored the basal firing rate from an average of 14±1Hz (n=2 animals, 100 cells) to nearly normal levels of 32±2Hz (n=2 animals, 72 cells; **Fig 4C, 4D**). As in the *MIM*^{EX15} mutants, the firing rate reached maximal effect at 5-6 hours of SFK inhibition (**SI Appendix Fig S3**), leading us to conclude that inappropriate SFK activity underlies both the *ATXN2* and *MTSS1*-mediated firing phenotype.

The convergence of *Mtss1* and *ATXN2* on SFK activity suggested they work in a common or parallel molecular pathway. To distinguish between these possibilities, we further interrogated *MTSS1* protein levels in *ATXN2*^{Q127} cerebella. While we found reduction of *MTSS1* protein (**Fig S4A**) and RNA in *ATXN2*^{Q127} Purkinje neurons (**Fig S4B**), we failed to see comparable changes in *ATXN2* levels in 4-week old *MIM*^{EX15} mice (**Fig 4E**). Because *ATXN2* possesses RNA binding activity, and *Mtss1* contains a long 3'UTR, we hypothesized that *ATXN2* controls *Mtss1* translation in Purkinje neurons. RNA-IP followed by QPCR in cells expressing tagged versions of either WT (*ATXN*^{Q22}) or SCA2 (*ATXN2*^{Q108}) demonstrated both proteins specifically bound *MTSS1* mRNA compared to *GAPDH* control. (**Fig 4F**). Using a luciferase reporter fused to the *MTSS1* 3' UTR we were able to map the *ATXN2* interacting domain to a central 500bp region that was sufficient for both RNA-protein interaction and translation control (**SI Appendix Fig S4C,D**). Furthermore, polyribosome fractionation experiments revealed that pathogenic *ATXN2*^{Q108} was sufficient to block the translation of reporter mRNA fused to the *MTSS1* 3'UTR shifting the transcript from the polyribosome fractions to a detergent resistant fraction consistent with stress granules (**Fig 4G**). These results suggest the pathogenic *ATXN2* acts directly as a dominant negative RNA binding protein preventing *MTSS1* translation. Notably, we observed *MTSS1* abundance is reduced in human SCA patient cerebellum, bolstering the evolutionary conservation of the *ATXN2*/*MTSS1* interaction (**Fig 4H**).

SFK inhibition rescues Purkinje neuron firing across SCA

Two other SCA mouse models have been shown to have slow basal firing rates, SCA1 (2) and SCA5 (3). Much like SCA2, SCA1 is due to a polyQ expansion in the RNA binding protein ATAXIN-1 (ATXN1)(71). One observed result of the SCA1 allele is changed ATXN1 association with transcriptional regulatory complexes (72), leading to vastly different Purkinje neuron mRNA profiles (73). However, the exact targets that drive SCA1 pathogenesis are still being determined. Unlike SCA1 and SCA2, SCA5 is a more pure cerebellar ataxia due to lesions in the structural protein β -III spectrin (13). β -III spectrin directly binds to and controls the cell membrane localization of EAAT4 (excitatory amino acid transporter 4), a protein involved in the synaptic clearance of glutamate (12, 74).

If SCA1 or SCA5 arises similarly to SCA2 by dysregulation of the MTSS1/SFK cassette, we would expect decreased MTSS1 abundance. Indeed, in the *ATXN1^{Q82}* mouse model of SCA1 (75) we observed a 95% decrease in MTSS1 protein abundance (**Fig 5A**) with only a 50% reduction in calbindin, suggesting the loss of MTSS1 is not solely due to loss of Purkinje neurons.

Atxn1 pathogenicity is partially driven by phosphorylation at serine 776 (72), which was unchanged in 4-week old *MIM^{EX15}* mice, suggesting MTSS1 is a target of the SCA1 allele (**Fig 5B**). Additionally, *Mtss1* transcript abundance is reduced at multiple ages in *ATXN1^{Q82}* mice (73) (**Fig 5C**). We found treating *ATXN1^{Q82}* slices with dasatinib increased the basal firing rate from a baseline of 15 \pm 1Hz (n=3 animals, 21 cells) to 23 \pm 2Hz (n=3 animals, 21 cells), a level statistically indistinguishable from dasatinib-treated controls (**Fig 5D**).

By contrast, the *Sptbn2* knockout model of SCA5 (β III^{-/-})(3), showed no change in MTSS1 protein abundance at 3 weeks yet demonstrated a clear increase in SFK^{Y416} phosphorylation (**Fig 5E**). We also observe increased basal firing from 25 \pm 1Hz (n=2 animals, 31 cells) to 30 \pm 2Hz (n=3 animals, 43 cells) over a 7-hour period of dasatinib treatment (**Fig 5F**). We fail to see changes in β -III spectrin abundance in *MIM^{EX15}* mice, and detect a 40% decrease in β -III spectrin levels in 24-week *ATXN2^{Q127}* mice that is likely due to reduced Purkinje neuron dendritic arbor size, correlating with calbindin levels (**Fig 5G, 5H**). Together these data suggest that β -III spectrin and MTSS1 may work in parallel, through different mechanisms, to modulate SFK activity (**Fig 5I**).

Discussion

While SCA gene functions appear heterogeneous, our study establishes a genetic framework to understand how several SCA loci regulate SFK activity to ensure

neuronal homeostasis and survival. We identify β -III spectrin and MTSS1, proteins that link the cell membrane and actin cytoskeleton, as negative regulators of Src family kinases. We show that MTSS1 is a target of the SCA genes *ATXN1* and *ATXN2* (**Fig 5I**), and that increased SFK activity from lesions in *MTSS1*, *SPTNB2* (SCA5), *ATXN1*(SCA1), and *ATXN2* (SCA2) reduces Purkinje neuron basal firing, an endophenotype that underlies multiple ataxias, providing support for the clinical use of SFK inhibitors in many SCA patients.

Our results reveal a central role for the MTSS1/SFK regulatory cassette in controlling neuronal homeostasis and survival. MTSS1 regulation of SFKs has been demonstrated in several migratory cell types including metastatic breast cancer and *Drosophila* border cells. This is the first demonstration of the regulatory cassette functioning in non-migratory post-mitotic cells. MTSS1 integrates the cell membrane and cytoskeletal response to local signals by serving as a docking site for the kinases and phosphatases that control actin polymerization (76), a process essential for dendritic spine assembly, maintenance and function. In fly border cells, MTSS1-regulated SFK activity polarizes the membrane to spatially detect guidance cues. Similarly, MTSS1 functions in neurons to promote dendritic arborization and spine formation, structures that were shown to be essential for maintaining basal firing frequencies by electrically isolating increasing areas of Purkinje neuron dendrites (59). Other members of the I-BAR family of membrane/cytoskeletal signaling proteins have been implicated in human neurological disorders such as microcephaly (77), but it remains to be determined how they interact with MTSS1.

Disruption of post-transcriptional gene regulation leading to altered proteostasis has recently emerged as a key contributor to neurodegeneration. In the cerebellum, reducing the abundance of the RNA-binding protein Pumilio leads to SCA1-like neurodegeneration through a specific increase in *ATXN1* protein levels (78, 79). Yet Pumilio binds hundreds of transcripts to control protein levels (80, 81), suggesting that changing protein abundance of a few key effector genes post-transcriptionally leads to disease. Our data demonstrate that *MTSS1* is a key effector gene whose activity is tightly regulated to prevent Purkinje neuron malfunction. Post-transcriptional control of *MTSS1* is disrupted in many disease states such as cancer, where *MTSS1* levels are reduced by locus deletion or miRNA overexpression and are associated with increased metastasis and poorer prognosis (67, 82). In Purkinje neurons, the SCA1 *ATXN1*^{Q82} allele reduces *MTSS1* transcript levels. *ATXN1* is thought to act as a transcriptional

regulator by associating with the transcriptional repressor *Capicua* (CIC) (72), though it remains to be shown whether the ATXN1/CIC complex occupies the *MTSS1* promoter. By contrast, the SCA2 allele ATXN2^{Q58} binds the MTSS1 3' UTR to prevent ribosome binding and MTSS1 translation, ultimately leading to increased SFK activity. ATXN2 (and the redundant gene ATXN2L) have recently been identified in a large complex of 3' UTR binding proteins that regulate networks of genes controlling epithelial differentiation and homeostasis (83). Our results suggest other ataxia disease genes that control proteostasis may also regulate MTSS1 abundance, and the strong role for miRNAs controlling MTSS1 abundance in cancer suggest they may also function as effectors of as yet undescribed ataxia loci.

The identification of the MTSS1/SFK regulatory cassette in multiple ataxias further reinforces the pathological consequences associated with inappropriate SFK activation in response to a variety of cellular stresses. While the cytoskeletal regulator MTSS1 is an evolutionarily-conserved SFK inhibitor, SFK effects on Purkinje neuron basal firing may derive from the fundamental roles SFKs play in cell homeostasis outside cytoskeletal control. For example, SFK control of translation is implicated in Alzheimer disease, as reducing SFK activity proves beneficial for Alzheimer disease progression (24) due to SFK control of pathogenic A β translation (84). SFK impairment of autophagy is seen in models of Amyotrophic lateral sclerosis and Duchenne muscular dystrophy (23, 85). Additionally, reduction of Src kinase expression was identified as a suppressor of SCA1 toxicity in *Drosophila* ommatidia (86), supporting the need for moderating SFK activity. The pleiotropic effects of inappropriate SFK activity suggest that SFK inhibition may be a critical therapeutic node to slow the progression of multiple neurodegenerative disorders including SCAs. Our work points out the need for future development of neuro-active SFK inhibitor variants, as currently approved Src inhibitors were designed for oncology targets and lack potent central nervous system activity. Further, while we provide data for kinase inhibition to suppress MTSS1 loss, we have previously shown that SFK regulation by regulatory receptor tyrosine phosphatases, or deletion of endocytic adapter proteins can also revert the effects of MTSS1 loss. Given the challenge of developing specific kinase inhibitors, our work opens additional therapeutic classes to alleviate the progression of neurodegenerative diseases.

In summary, the identification of *Mtss1* as a novel recessive ataxia locus extends the physiologic functions requiring the MTSS1/SFK signaling cassette, which include cell polarity, migration, and cancer metastasis. Each of these disparate processes highlight

the common role MTSS1 plays integrating the cell membrane and cytoskeletal response to local signals, as the dendritic spine defects seen in *MIM^{EX15}*-mutant Purkinje neurons (**Fig 3A-E**) recalls the loss of directional cell extensions in migrating *Drosophila* border cells (29). They also reinforce the critical need to suppress inappropriate SFK activity, and provide a therapeutic opportunity for otherwise devastating and debilitating diseases.

Author Contributions

AEO and SXA conceived the project. ASB, SXA, BA, JM performed and interpreted most experiments. PM performed and interpreted all electrophysiology in *Mtss1^{EX15}* and *ATXN2^{Q127}* mice. EP and MJ performed and interpreted all electrophysiology and western blots in β III-spectrin^{-/-} mice. RC, HH and VS performed and interpreted all electrophysiology and western blots in *ATXN1^{Q82}* mice. SP and DS performed and interpreted MTSS1 western blot and QPCR in *ATXN2^{Q127}* mice and HEK-293 cell RNAIP. SP performed and interpreted MTSS1 staining in human samples. ET quantified biocytin-filled Purkinje data. TSO and SMP contributed ideas and interpreted results. ASB and AEO wrote the manuscript with input from all authors.

Acknowledgements

The authors would like to acknowledge JoAnn Buchanan for assistance with TEM microscopy, Hak Kyun Kim, Miguel Mata, Peter Sarnow for assistance with ribosome profiling, and SBNFL for assistance with behavior assays. **Funding:** Oro R01 AR052785, Brown F32 GM105227, Otis R01 NS090930, Jackson The Wellcome Trust 093077

References

1. Hansen ST, Meera P, Otis TS, Pulst SM (2013) Changes in Purkinje cell firing and gene expression precede behavioral pathology in a mouse model of SCA2. *Human Molecular Genetics* 22(2):271–283.
2. Inoue T, et al. (2001) Calcium dynamics and electrophysiological properties of cerebellar Purkinje cells in SCA1 transgenic mice. *J Neurophysiol* 85(4):1750–1760.
3. Perkins EM, et al. (2010) Loss of β -III Spectrin Leads to Purkinje Cell Dysfunction Recapitulating the Behavior and Neuropathology of Spinocerebellar Ataxia Type 5 in Humans. *Journal of Neuroscience* 30(14):4857–4867.
4. Hourez R, et al. (2011) Aminopyridines Correct Early Dysfunction and Delay Neurodegeneration in a Mouse Model of Spinocerebellar Ataxia Type 1. *Journal of Neuroscience* 31(33):11795–11807.

- 455 5. Dell'Orco JM, et al. (2015) Neuronal Atrophy Early in Degenerative Ataxia Is a
456 Compensatory Mechanism to Regulate Membrane Excitability. *J Neurosci*
457 35(32):11292–11307.
- 458 6. Nakamura K, et al. (2001) SCA17, a novel autosomal dominant cerebellar ataxia
459 caused by an expanded polyglutamine in TATA-binding protein. *Human Molecular*
460 *Genetics* 10(14):1441–1448.
- 461 7. Dansithong W, et al. (2015) Ataxin-2 Regulates RGS8 Translation in a New BAC-
462 SCA2 Transgenic Mouse Model. *PLoS Genet* 11(4):e1005182–29.
- 463 8. Doss-Pepe EW, Stenroos ES, Johnson WG, Madura K (2003) Ataxin-3
464 Interactions with Rad23 and Valosin-Containing Protein and Its Associations with
465 Ubiquitin Chains and the Proteasome Are Consistent with a Role in Ubiquitin-
466 Mediated Proteolysis. *Molecular and Cellular Biology* 23(18):6469–6483.
- 467 9. Burnett B (2003) The polyglutamine neurodegenerative protein ataxin-3 binds
468 polyubiquitylated proteins and has ubiquitin protease activity. *Human Molecular*
469 *Genetics* 12(23):3195–3205.
- 470 10. Iwaki A, et al. (2007) Heterozygous deletion of ITPR1, but not SUMF1, in
471 spinocerebellar ataxia type 16. *Journal of medical genetics* 45(1):32–35.
- 472 11. Marelli C, et al. (2011) SCA15 due to large ITPR1 deletions in a cohort of 333
473 white families with dominant ataxia. *Archives of neurology* 68(5):637–643.
- 474 12. Jackson M, et al. (2001) Modulation of the neuronal glutamate transporter EAAT4
475 by two interacting proteins. *Nature* 410(6824):89–93.
- 476 13. Ikeda Y, et al. (2006) Spectrin mutations cause spinocerebellar ataxia type 5. *Nat*
477 *Genet* 38(2):184–190.
- 478 14. Soriano P, Montgomery C, Geske R, Bradley A (1991) Targeted disruption of the
479 c-src proto-oncogene leads to osteopetrosis in mice. *Cell* 64(4):693–702.
- 480 15. Stein PL, Vogel H, Soriano P (1994) Combined deficiencies of Src, Fyn, and Yes
481 tyrosine kinases in mutant mice. *Genes & Development* 8(17):1999–2007.
- 482 16. Grant SG, et al. (1992) Impaired long-term potentiation, spatial learning, and
483 hippocampal development in fyn mutant mice. *Science* 258(5090):1903–1910.
- 484 17. Grant SG, Karl KA, Kiebler MA, Kandel ER (1995) Focal adhesion kinase in the
485 brain: novel subcellular localization and specific regulation by Fyn tyrosine kinase
486 in mutant mice. *Genes & Development* 9(15):1909–1921.
- 487 18. Kuo G (2005) Absence of Fyn and Src Causes a Reeler-Like Phenotype. *Journal*
488 *of Neuroscience* 25(37):8578–8586.
- 489 19. Okada M, Nada S, Yamanashi Y, Yamamoto T, Nakagawa H (1991) CSK: a
490 protein-tyrosine kinase involved in regulation of src family kinases. *Journal of*
491 *Biological Chemistry* 266(36):24249–24252.

- 492 20. Zheng XM, Wang Y, Pallen CJ (1992) Cell transformation and activation of pp60c-
493 src by overexpression of a protein tyrosine phosphatase. *Nature* 359(6393):336–
494 339.
- 495 21. Kapus A, Szászi K, Sun J, Rizoli S, Rotstein OD (1999) Cell shrinkage regulates
496 Src kinases and induces tyrosine phosphorylation of cortactin, independent of the
497 osmotic regulation of Na⁺/H⁺ exchangers. *Journal of Biological Chemistry*
498 274(12):8093–8102.
- 499 22. Lu YM, Roder JC, Davidow J, Salter MW (1998) Src activation in the induction of
500 long-term potentiation in CA1 hippocampal neurons. *Science* 279(5355):1363–
501 1367.
- 502 23. Imamura K, et al. (2017) The Src/c-Abl pathway is a potential therapeutic target in
503 amyotrophic lateral sclerosis. *Sci Transl Med* 9(391):eaaf3962.
- 504 24. Kaufman AC, et al. (2015) Fyn inhibition rescues established memory and
505 synapse loss in Alzheimer mice. *Ann Neurol* 77(6):953–971.
- 506 25. Pal R, et al. (2014) Src-dependent impairment of autophagy by oxidative stress in
507 a mouse model of Duchenne muscular dystrophy. *Nature Communications* 5:1–
508 10.
- 509 26. Lee Y-G, Macoska JA, Korenchuk S, Pienta KJ (2002) MIM, a Potential
510 Metastasis Suppressor Gene in Bladder Cancer. *Neoplasia* 4(4):291–294.
- 511 27. Yang C, Hoelzle M, Disanza A, Scita G, Svitkina T (2009) Coordination of
512 Membrane and Actin Cytoskeleton Dynamics during Filopodia Protrusion. *PLoS*
513 *ONE* 4(5):e5678–9.
- 514 28. Bershteyn M, Atwood SX, Woo W-M, Li M, Oro AE (2010) MIM and Cortactin
515 Antagonism Regulates Ciliogenesis and Hedgehog Signaling. 19(2):270–283.
- 516 29. Quinones GA, Jin J, Oro AE (2010) I-BAR protein antagonism of endocytosis
517 mediates directional sensing during guided cell migration. *The Journal of Cell*
518 *Biology* 189(2):353–367.
- 519 30. Callahan CA, et al. (2004) MIM/BEG4, a Sonic hedgehog-responsive gene that
520 potentiates Gli-dependent transcription. *Genes & Development* 18(22):2724–
521 2729.
- 522 31. Ohnishi H, Murata Y, Okazawa H, Matozaki T (2011) Src family kinases:
523 modulators of neurotransmitter receptor function and behavior. *Trends in*
524 *Neurosciences* 34(12):629–637.
- 525 32. Uruno T, et al. (2001) Activation of Arp2/3 complex-mediated actin polymerization
526 by cortactin. *Nat Cell Biol* 3(3):259–266.
- 527 33. Wu H, Parsons JT (1993) Cortactin, an 80/85-kilodalton pp60src substrate, is a
528 filamentous actin-binding protein enriched in the cell cortex. *The Journal of Cell*
529 *Biology* 120(6):1417–1426.

- 530 34. Huang C, et al. (1997) Down-regulation of the filamentous actin cross-linking
531 activity of cortactin by Src-mediated tyrosine phosphorylation. *Journal of*
532 *Biological Chemistry* 272(21):13911–13915.
- 533 35. Lynch DK, et al. (2003) A Cortactin-CD2-associated Protein (CD2AP) Complex
534 Provides a Novel Link between Epidermal Growth Factor Receptor Endocytosis
535 and the Actin Cytoskeleton. *Journal of Biological Chemistry* 278(24):21805–
536 21813.
- 537 36. Hensel N, Claus P (2018) The Actin Cytoskeleton in SMA and ALS: How Does It
538 Contribute to Motoneuron Degeneration? *The Neuroscientist* 24(1):54–72.
- 539 37. Yan Z, Kim E, Datta D, Lewis DA, Soderling SH (2016) Synaptic Actin
540 Dysregulation, a Convergent Mechanism of Mental Disorders? *Journal of*
541 *Neuroscience* 36(45):11411–11417.
- 542 38. Avery AW, Thomas DD, Hays TS (2017) β -III-spectrin spinocerebellar ataxia type
543 5 mutation reveals a dominant cytoskeletal mechanism that underlies dendritic
544 arborization. *Proceedings of the National Academy of Sciences* 114(44):E9376–
545 E9385.
- 546 39. Yu D, et al. (2011) Mice deficient in MIM expression are predisposed to
547 lymphomagenesis. 31(30):3561–3568.
- 548 40. Saarikangas J, et al. (2011) Missing-in-metastasis MIM/MTSS1 promotes actin
549 assembly at intercellular junctions and is required for integrity of kidney epithelia.
550 *Journal of Cell Science* 124(8):1245–1255.
- 551 41. Saarikangas J, et al. (2015) MIM-Induced Membrane Bending Promotes Dendritic
552 Spine Initiation. *Developmental Cell*:1–17.
- 553 42. Glassmann A, et al. (2007) Developmental expression and differentiation-related
554 neuron-specific splicing of metastasis suppressor 1 (Mtss1) in normal and
555 transformed cerebellar cells. *BMC Dev Biol* 7(1):111–15.
- 556 43. Nixdorf S, et al. (2004) Expression and regulation of MIM (Missing In Metastasis),
557 a novel putative metastasis suppressor gene, and MIM-B, in bladder cancer cell
558 lines. *Cancer Letters* 215(2):209–220.
- 559 44. Sistig T (2017) Mtss1 promotes maturation and maintenance of cerebellar
560 neurons via splice variant-specific effects. *Brain Structure and Function* 0(0):0–0.
- 561 45. Fahrenkamp D, Herrmann O, Koschmieder S, Brummendorf TH, Schemionek M
562 (2017) Mtss1(CSC156) mutant mice fail to display efficient Mtss1 protein
563 depletion. *Nature Publishing Group*:1–3.
- 564 46. Guyenet SJ, et al. (2010) A Simple Composite Phenotype Scoring System for
565 Evaluating Mouse Models of Cerebellar Ataxia. *JoVE* (39):1–3.
- 566 47. Dawson JC, Timpson P, Kalna G, Machesky LM (2011) Mtss1 regulates
567 epidermal growth factor signaling in head and neck squamous carcinoma cells.

- 568 31(14):1781–1793.
- 569 48. Hara T, et al. (2006) Suppression of basal autophagy in neural cells causes
570 neurodegenerative disease in mice. *Nature* 441(7095):885–889.
- 571 49. Komatsu M, et al. (2006) Loss of autophagy in the central nervous system causes
572 neurodegeneration in mice. *Nature* 441(7095):880–884.
- 573 50. Kegel KB, et al. (2000) Huntingtin expression stimulates endosomal-lysosomal
574 activity, endosome tubulation, and autophagy. *J Neurosci* 20(19):7268–7278.
- 575 51. Nixon RA, et al. (2005) Extensive involvement of autophagy in Alzheimer disease:
576 an immuno-electron microscopy study. *Journal of Neuropathology and*
577 *Experimental Neurology* 64(2):113–122.
- 578 52. Nascimento-Ferreira I, et al. (2011) Overexpression of the autophagic beclin-1
579 protein clears mutant ataxin-3 and alleviates Machado–Joseph disease. *Brain*
580 134(5):1400–1415.
- 581 53. Ropolo A, et al. (2007) The pancreatitis-induced vacuole membrane protein 1
582 triggers autophagy in mammalian cells. *Journal of Biological Chemistry*
583 282(51):37124–37133.
- 584 54. Gal J, Ström A-L, Kilty R, Zhang F, Zhu H (2007) p62 Accumulates and Enhances
585 Aggregate Formation in Model Systems of Familial Amyotrophic Lateral Sclerosis.
586 *Journal of Biological Chemistry* 282(15):11068–11077.
- 587 55. Shakkottai VG, et al. (2011) Early Changes in Cerebellar Physiology Accompany
588 Motor Dysfunction in the Polyglutamine Disease Spinocerebellar Ataxia Type 3.
589 *Journal of Neuroscience* 31(36):13002–13014.
- 590 56. Canepari M, Ogden D (2003) Evidence for protein tyrosine phosphatase, tyrosine
591 kinase, and G-protein regulation of the parallel fiber metabotropic slow EPSC of
592 rat cerebellar Purkinje neurons. *J Neurosci* 23(10):4066–4071.
- 593 57. Walter JT, Alviña K, Womack MD, Chevez C, Khodakhah K (2006) Decreases in
594 the precision of Purkinje cell pacemaking cause cerebellar dysfunction and ataxia.
595 *Nat Neurosci* 9(3):389–397.
- 596 58. Cerminara NL, Rawson JA (2004) Evidence that climbing fibers control an intrinsic
597 spike generator in cerebellar Purkinje cells. *J Neurosci* 24(19):4510–4517.
- 598 59. Womack M, Khodakhah K (2002) Active contribution of dendrites to the tonic and
599 trimodal patterns of activity in cerebellar Purkinje neurons. *J Neurosci*
600 22(24):10603–10612.
- 601 60. Meera P, Pulst S, Otis T (2017) A positive feedback loop linking enhanced mGluR
602 function and basal calcium in spinocerebellar ataxia type 2. *Elife* 6:19854.
- 603 61. Porkka K, et al. (2008) Dasatinib crosses the blood-brain barrier and is an efficient
604 therapy for central nervous system Philadelphia chromosome-positive leukemia.

- 605 *Blood* 112(4):1005–1012.
- 606 62. Pulst SM, et al. (1996) Moderate expansion of a normally biallelic trinucleotide
607 repeat in spinocerebellar ataxia type 2. *Nat Genet* 14(3):269–276.
- 608 63. Huynh DP, Maalouf M, Silva AJ, Schweizer FE, Pulst SM (2009) Dissociated fear
609 and spatial learning in mice with deficiency of ataxin-2. *PLoS ONE* 4(7):e6235.
- 610 64. Elden AC, et al. (2010) Ataxin-2 intermediate-length polyglutamine expansions
611 are associated with increased risk for ALS. *Nature* 466(7310):1069–1075.
- 612 65. Lim C, Allada R (2013) ATAXIN-2 Activates PERIOD Translation to Sustain
613 Circadian Rhythms in *Drosophila*. *Science* 340(6134):875–879.
- 614 66. Xu X, et al. (2014) Anti-miR182 Reduces Ovarian Cancer Burden, Invasion, and
615 Metastasis: An In Vivo Study in Orthotopic Xenografts of Nude Mice. *Molecular*
616 *Cancer Therapeutics* 13(7):1729–1739.
- 617 67. Wu W, et al. (2014) MicroRNA-135b regulates metastasis suppressor 1
618 expression and promotes migration and invasion in colorectal cancer. *Mol Cell*
619 *Biochem* 388(1-2):249–259.
- 620 68. Zhou W, et al. (2012) MiR-135a promotes growth and invasion of colorectal
621 cancer via metastasis suppressor 1 in vitro. *Acta biochimica et biophysica Sinica*
622 44(10):838–846.
- 623 69. Kedmi M, et al. (2015) EGF induces microRNAs that target suppressors of cell
624 migration: miR-15b targets MTSS1 in breast cancer. *Science Signaling*
625 8(368):ra29–ra29.
- 626 70. Jahid S, et al. (2012) miR-23a Promotes the Transition from Indolent to Invasive
627 Colorectal Cancer. *Cancer Discovery* 2(6):540–553.
- 628 71. Orr HT, et al. (1993) Expansion of an unstable trinucleotide CAG repeat in
629 spinocerebellar ataxia type 1. *Nat Genet* 4(3):221–226.
- 630 72. Lam YC, et al. (2006) ATAXIN-1 Interacts with the Repressor Capicua in Its
631 Native Complex to Cause SCA1 Neuropathology. *Cell* 127(7):1335–1347.
- 632 73. Ingram M, et al. (2016) Cerebellar Transcriptome Profiles of ATXN1 Transgenic
633 Mice Reveal SCA1 Disease Progression and Protection Pathways. *Neuron*
634 89(6):1194–1207.
- 635 74. Lise S, et al. (2012) Recessive Mutations in SPTBN2 Implicate β -III Spectrin in
636 Both Cognitive and Motor Development. *PLoS Genet* 8(12):e1003074–14.
- 637 75. Burright EN, et al. (1995) SCA1 transgenic mice: a model for neurodegeneration
638 caused by an expanded CAG trinucleotide repeat. *Cell* 82(6):937–948.
- 639 76. Gonzalez-Quevedo R, Shoffer M, Horng L, Oro AE (2005) Receptor tyrosine
640 phosphatase-dependent cytoskeletal remodeling by the hedgehog-responsive

- gene MIM/BEG4. *The Journal of Cell Biology* 168(3):453–463.
77. Alazami AM, et al. (2015) Accelerating Novel Candidate Gene Discovery in Neurogenetic Disorders via Whole-Exome Sequencing of Prescreened Multiplex Consanguineous Families. *CellReports* 10(2):148–161.
 78. Gennarino VA, et al. (2015) Pumilio1 Haploinsufficiency Leads to SCA1-like Neurodegeneration by Increasing Wild-Type Ataxin1 Levels. *Cell* 160(6):1087–1098.
 79. Gennarino VA, et al. (2018) A Mild PUM1 Mutation Is Associated with Adult-Onset Ataxia, whereas Haploinsufficiency Causes Developmental Delay and Seizures. *Cell* 172(5):924–932.e11.
 80. Chen D, et al. (2012) Pumilio 1 Suppresses Multiple Activators of p53 to Safeguard Spermatogenesis. *Current Biology* 22(5):420–425.
 81. Kedde M, et al. (2010) A Pumilio-induced RNA structure switch in p27-3' UTR controls miR-221 and miR-222 accessibility. *Nature Publishing Group* 12(10):1014–1020.
 82. Lei R, et al. (2013) Suppression of MIM by microRNA-182 activates RhoA and promotes breast cancer metastasis. 33(10):1287–1296.
 83. Wang Y, Arribas-Layton M, Chen Y, Lykke-Andersen J, Sen GL (2015) DDX6 Orchestrates Mammalian Progenitor Function through the mRNA Degradation and Translation Pathways. *Molecular Cell* 60(1):118–130.
 84. Li C, Götz J (2017) Somatodendritic accumulation of Tau in Alzheimer's disease is promoted by Fyn- mediated local protein translation. *The EMBO Journal* 36(21):3120–3138.
 85. Pal R, et al. (2014) Src-dependent impairment of autophagy by oxidative stress in a mouse model of Duchenne muscular dystrophy. *Nature Communications* 5:1–10.
 86. Park J, et al. (2013) RAS-MAPK-MSK1 pathway modulates ataxin 1 protein levels and toxicity in SCA1. *Nature Publishing Group* 498(7454):325–331.
 87. Rodríguez CI, et al. (2000) High-efficiency deleter mice show that FLPe is an alternative to Cre-loxP. *Nat Genet* 25(2):139–140.
 88. Tang S-HE, Silva FJ, Tsark WMK, Mann JR (2002) A cre/loxP-deleter transgenic line in mouse strain 129S1/SvImJ. *genesis* 32(3):199–202.
 89. Zhang X-M, et al. (2004) Highly restricted expression of Cre recombinase in cerebellar Purkinje cells. *genesis* 40(1):45–51.

Figure Legends

Figure 1. *MIM*^{EX15} mutants develop progressive spinocerebellar ataxia

A: The structure of the *Mtss1* locus with alternative promoters and Src interacting domain deleted in *MIM*^{EX15} mutants. **B:** Loss of MTSS1 protein in *MIM*^{EX15} cerebellum lysate shown with MTSS1 antibody against N-terminal IMD domain. **C,D** *MIM*^{EX15} show slower movement velocity and reduced rearing frequency in open field tests. **E:** Impaired rotarod performance in *MIM*^{EX15} mutants shown as reduced duration (time to fall). **F:** A composite test of gait, balance, and grip strength to measure spinocerebellar ataxia symptoms. Increased score reflects reduced function with an age dependent increase in severity in *MIM*^{EX15} mutants. **G:** Age dependent loss of Purkinje neurons in *MIM*^{EX15} mutants occurs after the onset of ataxia. **H:** At 20 weeks *MIM*^{Loxp/-;Pcp2-Cre} and *MIM*^{Loxp/Loxp;Pcp2-Cre} mutants show dramatic reduction in Purkinje neurons that stain with MTSS1. Many Purkinje neurons persist, as there is a less dramatic reduction in calbindin positive Purkinje cell number. *p<0.05, **p<0.005, ***p<5E-5, one-way ANOVA with Tukey post-hoc test. ns not significant. Error bars, s.e.m.

Figure 2. *MIM*^{EX15} mutant Purkinje neurons undergo autophagy

A: *MIM*^{EX15} mutants display fused mitochondria shown by increased Complex 5 ATP-synthase immuno-staining and collapsed Golgi shown by reduced Giantin immune-staining at 4 weeks. **B:** 8 week old *MIM*^{EX15} mutants show increased LC3-II abundance (*P<0.005 student's t-test), **C:** *MIM*^{EX15} mutants show increased levels of mRNA for the autophagocytic marker *VMP1* (*p<0.05 student's t-test). **D:** *MIM*^{EX15} mutants show increased microglial infiltration shown by *Aif1* transcript. **E:** *MIM*^{EX15} mutants show GFAP⁺ glial infiltration during disease progression. **F:** Western blots quantifying increased cerebellar GFAP. **G:** *MIM*^{EX15} mutant cerebella do not have increased TUNEL stain at 4, 8 or 16 weeks of age.

Figure 3. *Mtss1* prevents SFK dependent firing defects and ataxia

A: Confocal projection of an individual Purkinje cell filled with biocytin and with fluorescent dye to visualize morphology (50µm, 5µm, 1µm scale bars). **B:** Measurement of dye filled Purkinje neurons show *MIM*^{EX15} mutants have reduced arbor volume (n=3 each genotype), **C:** reduced dendritic spine density, but **D:** no change in dendritic spine length and **E:** no change in dendritic spine width (*MIM*^{EX15/+} n=3, 1720 spines; *MIM*^{EX15} n=3, 1454 spines, *p<0.05 student's t-test). Error bars, s.e.m **F:** Western blot for active SFK-Y416 phosphorylation with actin loading control. Cerebellar lysate from *MIM*^{EX15} and age matched controls collected at indicated times between post-natal day 15 (P15) and

MTSS1/SFK Ataxia

post-natal day 30 (P30). **G:** Slow excitatory post synaptic potential (EPSP) spikes in wild type (WT) and *MIM^{EX15}* (top) elicited by stimulation of parallel fibers with 10 pulse trains at 100 Hz in the presence AMPA, NMDA and GABA receptor antagonists (control conditions). Corresponding intra-cellular Ca^{2+} signals ($\Delta\text{F}/\text{F}$) for responses for WT and *MIM^{EX15}* mGluR EPSPs are illustrated. EPSPs and corresponding Ca^{2+} signals are blocked by mGluR1 antagonist CPCCOEt (bottom). Summary data of intracellular Ca^{2+} signals ($\Delta\text{F}/\text{F}$) for responses for WT and *MTSS1^{EX15}* in control conditions and in presence of CPCCOEt are shown (right). **H:** Percent histograms of Purkinje neuron mean firing frequencies (left), examples of extracellular recording of 1 second duration of a spontaneously spiking Purkinje neuron in respective condition (center), and histograms of inter-spike intervals calculated for the 2 minute recording periods of the same neuron (right) are shown for WT, *MIM^{EX15}*, WT+dasatinib, or *MIM^{EX15}*+dasatinib conditions. **I:** Summary of data presented in H * $p=6.1\text{E-}14$ ** $p=1\text{E-}13$, one-way ANOVA, Tukey post-hoc **J:** Direct cerebellar administration of dasatinib maintains rotarod performance, slowing the progressive ataxia in *MIM^{EX15}* mice. $q=0.006$, two-stage step-up Benjamini, Krieger, Yekutieli method, Error bars, s.e.m.

Figure 4. MTSS1 is an Atxn2 translation target

A: Western blot of 24-week whole cerebellum lysate shows 90% reduction of upper band (arrow) that corresponds MTSS1 in *ATXN2^{Q127}* mice, while calbindin was reduced 50%. Actin is included as a loading control * $p<0.01$, ** $p<0.001$, Student's t-test. **B:** Western blot for active SFK-Y416 phosphorylation and total Src, with tubulin loading control using cerebellar lysate from 24 week *Atxn2^{Q127}* mice show 8-fold increase in SFK-Y416 abundance. **C:** Percent histograms of Purkinje neuron mean firing frequencies (left), examples of extracellular recording of 1 second duration of a spontaneously spiking Purkinje neuron in respective condition (center), and histograms of inter-spike intervals calculated for the 2 minute recording periods of the same neuron for *ATXN2^{Q127}* and *ATXN2^{Q127}*+dasatinib **D:** Mean firing rates ** $p=3.77\text{E-}8$, one-way ANOVA, Tukey post-hoc **E:** Western blot for Atxn2 with tubulin loading control. Cerebellar lysate from 4-week old *MIM^{EX15}* cerebellum and age matched controls. **F:** RNA-IP in HEK-293 cells for flag-*ATXN2^{Q22}* and flag-*ATXN2^{Q108}* show enrichment for *MTSS1* but not *GAPDH* mRNA, error bars are SD. **G:** Polyribosome fractionation in 293T cells transfected with *MTSS1*-UTR reporter and pCDNA, *ATXN2^{Q22}*, *ATXN2^{Q108}*, or *ATXN2^{Q22}*+*ATXN2^{Q108}*. Green line indicates UV254nm absorbance (nucleic acids) with 40S, 60S, 80S, polyribosome peaks

labeled. **H:** Remaining Purkinje neurons in human SCA2 cerebellum (Atxn2^{Q22/Q41}) show reduced MTSS1 staining compared to age matched control (Atxn2^{Q22/Q22}).

Figure 5. SFK dysregulation occurs in multiple SCA

A: Western blot of 15-week whole cerebellum lysate shows 95% reduction of upper band that corresponds MTSS1 in *ATXN1*^{Q82} mice with only a 50% reduction in calbindin. Tubulin is included as a loading control. **B:** Western blot of 4-week old *MIM*^{EX15} cerebellum lysate shows no change in phospho-Serine776 ATXN1 levels. **C:** RNA-seq from *ATXN1*^{Q82} cerebella show reduced FPKM for *Mtss1* mRNA in 12 and 28 week samples, * $q < 0.005$. **D:** Mean firing frequency values in Hz for WT and *ATXN1*^{Q82} mice, with and without dasatinib treatment. Error bars, s.e.m. (* $p = 0.0094$, one-way ANOVA with Tukey post-hoc) **E:** Western blot of 3-week whole cerebellum lysate shows no change MTSS1 in β III-spectrin^{-/-} mice, yet active SFK-Y416 phosphorylation is increased. Calbindin and total Src are included as a loading controls. **F:** SPTNB2 abundance is not changed in 4-week old *MIM*^{EX15} mice. **G:** β III-spectrin levels are reduced 40% in 24-week *ATXN2*^{Q127} mice. **H:** Mean firing frequency values in Hz for WT and β III-spectrin^{-/-} mice, with and without dasatinib treatment. Error bars, s.e.m. (* $p < 0.05$, 1-way ANOVA, Tukey posthoc) **I:** A model where pathogenic alleles of ATXN1 (*ATXN1*^{Q82}) and ATXN2 (*ATXN2*^{Q42}) prevent the accumulation of MTSS1 and SPTBN2 which restrain SFK activity to prevent abnormal firing patterns and neurodegeneration.

Supplementary Figure Legends

Figure S1 associated with Figure 1. Sagittal sections of *MIM*^{EX15} mutants and antibody validation **A:** mosaic images of 16 week old WT and *MIM*^{EX15} demonstrate widespread Purkinje neuron loss and increased GFAP staining intensity. **B:** MTSS1 antibody specificity is shown by lack of signal on *MIM*^{EX15} tissue. **C:** Western blot of 4 week cerebella show *MIM*^{EX15/+} have 25% reduction in MTSS1 compared to WT * $p < 0.05$, ** $p < 0.0001$, 1-way ANOVA, Tukey post-hoc test.

Figure S2, associated with Figure 2. Purkinje cell autophagy in *MIM*^{EX15} mutants

A: Western blot shows no increase in LC3-ii levels in 4 week old *MIM*^{EX15} mutants. **B:** *Sqstm1* (P62) transcript is not increased in *MIM*^{EX15} mutants and protein levels are not elevated. **C:** Electron micrographs of 8 week old animals showing defects present in 3 *MIM*^{EX15} mutants but absent in WT animals: swollen mitochondria where the inner

matrix is poorly resolved and dissociated from the outer matrix, electron dense autophagic bodies (AV), lamellar bodies in Purkinje neuron dendrites.

Figure S3, associated with Figures 3 and 4. Acute Src inhibition restores tonic firing rates

Average firing frequency measured at the end of each incubation hour of Dasatinib in MIM^{EX15} (A) and ATXN2^{Q127} (B) is plotted. A respective mean value with number of Purkinje neurons (PN) at indicated incubations is given in the figure. Note that baseline firing frequency of ATXN2^{Q127} (14±1 Hz, n=100 PNs) mice of this age is similar to the MIM^{EX15} (12±1 Hz, n=55 PNs). Basal firing frequency of PNs from wild type mouse are given.

Figure S4, associated with Figure 4. ATXN2 regulates translation through the MTSS1 3'UTR

A: MTSS1 immuno-fluorescence in ATXN2^{Q127} and age matched control mice show reduced Purkinje neuron signal at 4, 12 and 24 week time points. **B:** Quantitative RT-PCR (QPCR) shows *Mtss1* transcript abundance is reduced in ATXN2^{Q127} compared to age matched controls *p<0.05, **p< 0.01, student's t-test, SD error bars. **C:** RNA-IP followed by QPCR shows ATXN2 binding to the MTSS1 3'UTR is mediated by a central 500bp region *p< 0.05 **p=0.015, one-way ANOVA with Tukey post-hoc test. **D:** Luciferase reporter assay shows ATXN2 translation is strongly mediated by the 3'UTR, and ATXN2^{Q108} allele is sufficient to block activation ns not significant, all other interactions p<0.005. 2way ANOVA finds reporter constructs explain 56% of total variance, differences in response to transfection (pcDNA, ATXN2^{Q22}, ATXN2^{Q22+Q108}) between reporter constructs explains 30% of variance, and different response to transfection (pcDNA, ATXN2^{Q22}, ATXN2^{Q22+Q108}) within a reporter explain 14% of total variance.

808 *Further information and requests for resources and reagents should be directed to and*
809 *will be fulfilled by the Lead Contact, Anthony Oro (oro@stanford.edu)*

810 **Generation of MIM^{EX15} allele:**

811 To generate the MIM^{EX15} conditional allele exon15 was cloned into the PGK-gb2 targeting
812 vector between the 5' LoxP site and the 3' LoxP/FRT flanking neomycin cassette. The
813 targeting vector contained a 5.97kb 5' homology arm that included exons 12, 13, 14 and
814 a 2.34kb 3' homology arm that included the 3'-UTR. The targeting vector was
815 electroporated into C57bl6xSV129 embryonic stem cells, and Neo-resistant colonies
816 were screened by PCR. Chimeric mice were generated by injecting ES cells into
817 blastocysts, and chimeras were mated to a FLP deleter strain(87). To generate MIM^{EX15}
818 null animals, mice with the MIM^{EX15} conditional allele were crossed to HPRT-Cre
819 mice(88). Mice were maintained on a mixed C57bl6 SV129 background and examined at
820 listed ages.

821 **Western blot:**

822 Isolated tissues were lysed in RIPA buffer supplemented with complete mini protease
823 inhibitor (Roche) and PhosStop (Roche). Protein concentrations were normalized by
824 using the BCA assay (Pierce). Proteins were electrophoresed on Novex 4-12%, 3-8%,
825 10-20% gradient gels or 16% gels. Rabbit anti-Src-Y416 (CST 2101S or CST 6943S),
826 mouse anti-beta actin (Sigma), rabbit anti-Sptbn2 (Thermo PA1-46007), rabbit anti-Atnx2
827 (Sigma HPA021146), mouse anti-Atnx1 (abcam ab63376), rabbit anti-LC3A/B (CST
828 4108), rabbit anti-P62 (CST 23214) rabbit anti-Src (CST 2123 or CST 2108), primary
829 antibodies were detected with LICOR secondary antibodies.

830

831 **Antibodies and Immunofluorescence:**

832 Isolated cerebella were immersion fixed in 4% paraformaldehyde and embedded in
833 paraffin. 7µm sections were cut and deparaffinized using standard conditions before
834 staining. Sections were blocked with 20% horse serum 0.3% Triton X-100 in PBS. The
835 following antibodies were used at 1:1000 dilutions:

836 Rabbit anti-Mtss1(30), Rabbit anti-Calbindin (CST 13176), mouse anti-Calbindin-D-28K
837 monoclonal (Sigma), mouse anti-Complex V (Novex 459240), rabbit anti-Ubiquitin (CST
838 3933), rabbit anti-Giantin (Abcam ab 24586), Chicken anti-GFAP (Abcam ab4674).

839 Alexafluor conjugated secondary antibodies were purchased from Invitrogen. Images

were acquired either on a Leica SP2 AOBS laser scanning microscope or a Zeiss axioplan widefield scope.

Human samples:

Paraffin-embedded brain slices from SCA2 patient were provided by Prof. Arnulf H. Koeppen, M.D., Albany Medical College, New York, USA. Non-SCA2 control paraffin-embedded brain slices were provided by Dr. Sonnen, Pathologist, University of Utah. Human tissues were maintained and processed under standard conditions consistent with National Institutes of Health guidelines and conformed to an approved University of Utah IRB protocol. Sections were deparaffinized using standard conditions and blocked/permeabilized with 5% donkey serum 0.3% Triton X-100 in PBS and processed for immunostaining. The nuclei were stained with DAPI followed by mounting with Fluoromount-G (Southern Biotech, Cat# 0100-01). Antibody dilutions for tissue immunostainings were custom-designed MTSS1 antibody (1: 500) and fluorescent secondary antibody: goat anti-rabbit IgG (H+L) antibody, DyLight-488 [(1:1,000) (ThermoFisher Scientific, Cat# 35552)]. Images were acquired using confocal microscope (Nikon Eclipse Ti microscopy) in University of Utah cell imaging core lab, and analyzed by NIS-Elements AR 4.5 software. As massive degeneration of cerebellum is seen in SCA2 brain tissue, the lobe can't be verifiable.

Electrophysiology:

Preparation of Cerebellar Slices (SCA2 and Mtss1)

Acute parasagittal slices of 285µm thickness were prepared from the cerebella of 4- to 8-week-old mutant and control littermates following published methods(1). In brief, brains were removed quickly and immersed in an ice-cold artificial cerebrospinal fluid (ACSF or extracellular) solution consisting of: 119 mM NaCl, 26 mM NaHCO₃, 11 mM glucose, 2.5 mM KCl, 2.5 mM CaCl₂, 1.3 mM MgCl₂ and 1 mM NaH₂PO₄, pH 7.4 when gassed with 5% CO₂ / 95% O₂. Cerebella were dissected and sectioned using a vibratome (Leica VT-1000). Slices were initially incubated at 35 °C for 35 min, and then at room temperature before recording in the same ACSF. Dasatinib (200nM) was added during cerebellar sectioning and remained on the slices for recording.

Recordings (SCA2 and Mtss1)

Non-invasive extracellular recordings were obtained from Purkinje neurons in voltage-clamp mode at 34.5 ± 1°C. The temperature was maintained using a dual channel

heater controller (Model TC-344B, Warner Instruments) and slices were constantly perfused with carbogen-bubbled extracellular solution alone or with 200 nM dasatinib. Cells were visualized with an upright Leica microscope using a water-immersion 40× objective. Glass pipettes were pulled with Model P-1000 (Sutter instruments). Pipettes had 1 to 3 MΩ resistance when filled with extracellular solution and were used to record action potential-associated capacitive current transients near Purkinje neuron axon hillock with the pipette potential held at 0 mV. Data was acquired at 20 kHz using a Multiclamp 700B amplifier, Digidata 1440 with pClamp10 (Molecular Devices), filtered at 4 kHz. A total of 50 to 100 Purkinje neurons were measured from each genotype and each recording was of 2 minutes in duration. The experimenter was blinded to the mouse genotype and 2 to 4 mice were used per genotype. Simultaneous mGluR EPSPs and calcium were measured in the presence of GABA_A receptor antagonist, picrotoxin (PTX at 100 μM), AMPA receptor blockers (5 μM NBQX and 10 μM DNQX) using a two-photon microscope and a standard electrophysiology set-up. The patch pipettes had 4 to 5 MΩ resistance when filled with internal solution (135 mM KMSO₄, NaCl, 10 mM HEPES, 3 mM MgATP, 0.3 mM Na₂GTP) containing 200 μM Oregon Green Bapta1 and 20 μM Alexa 594. The stimulating electrode was filled with ACSF containing 20 μM Alexa 594, placed in the dendritic region to minimally stimulate PF synaptic inputs. Slow mGluR EPSPs in control littermate and mutant were elicited by stimulation of PFs with 100 Hz trains, and 10 pulses in the presence of receptor antagonists that block AMPA, NMDA, GABA_A receptors. Corresponding intracellular Ca²⁺ signals (ΔF/F) for responses for wild type and mutant mGluR EPSPs were blocked by the mGluR1 antagonist CPCCOET.

Experiments were analyzed using both the Clampfit and Igor algorithms, and were further analyzed using Microsoft Excel. Figures were made in Igor program. Calcium signals were analyzed using Slidebook (Intelligent Imaging Innovations, Inc.). Results are presented as mean ±SEM. All chemicals were purchased either from Sigma Aldrich, Tocris and Invitrogen, USA.)

Biocytin fills of Purkinje neurons or Intracellular labeling of Purkinje neurons with Biocytin:

Biocytin filling of Purkinje neurons was performed using recording pipettes filled with 1% Biocytin (Tocris). Purkinje neurons were filled for 15 to 30 minutes and then the pipette was removed slowly for enabling the cell membrane to reseal. Slices were then fixed in

4% Paraformaldehyde overnight and washed 3 times with phosphate-buffered saline (PBS). Slices were then incubated with Alexa Fluor 488 streptavidin (1:500, Life S11223) in PBS, 0.5% Triton X-100, and 10% normal goat serum for 90min. After another 3 PBS washes, the slices were then mounted onto a slide with prolong gold. Individual biocytin-filled Purkinje cells were visualized on a Leica SP2 AOBS laser scanning microscope at a 0.5um step size. Dendritic arbor volume was measured by calculating the biocytin-filled area in each confocal optical section using ImageJ, adding the areas in each z-stack, and multiplying by the step size.

Figure 1

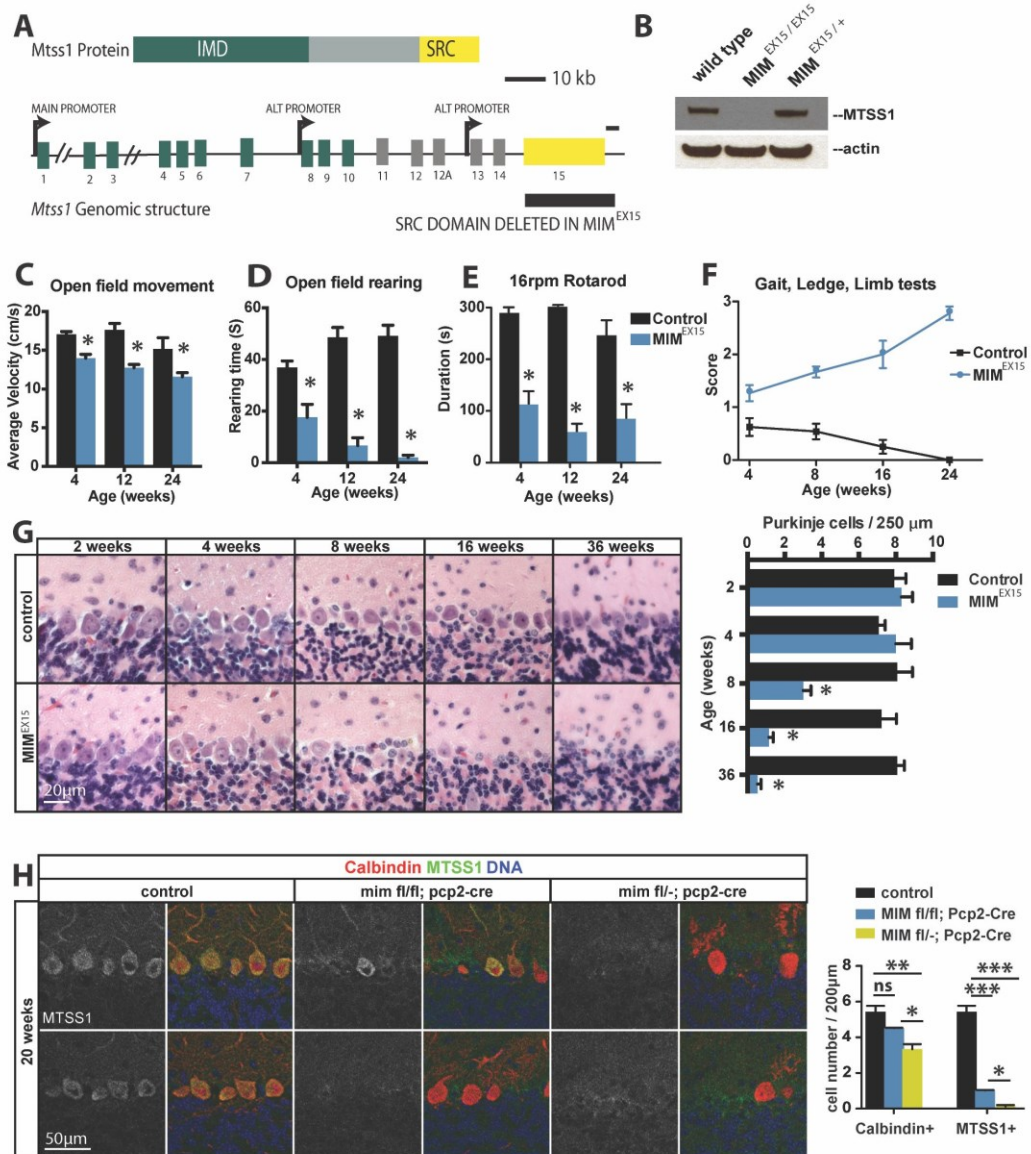
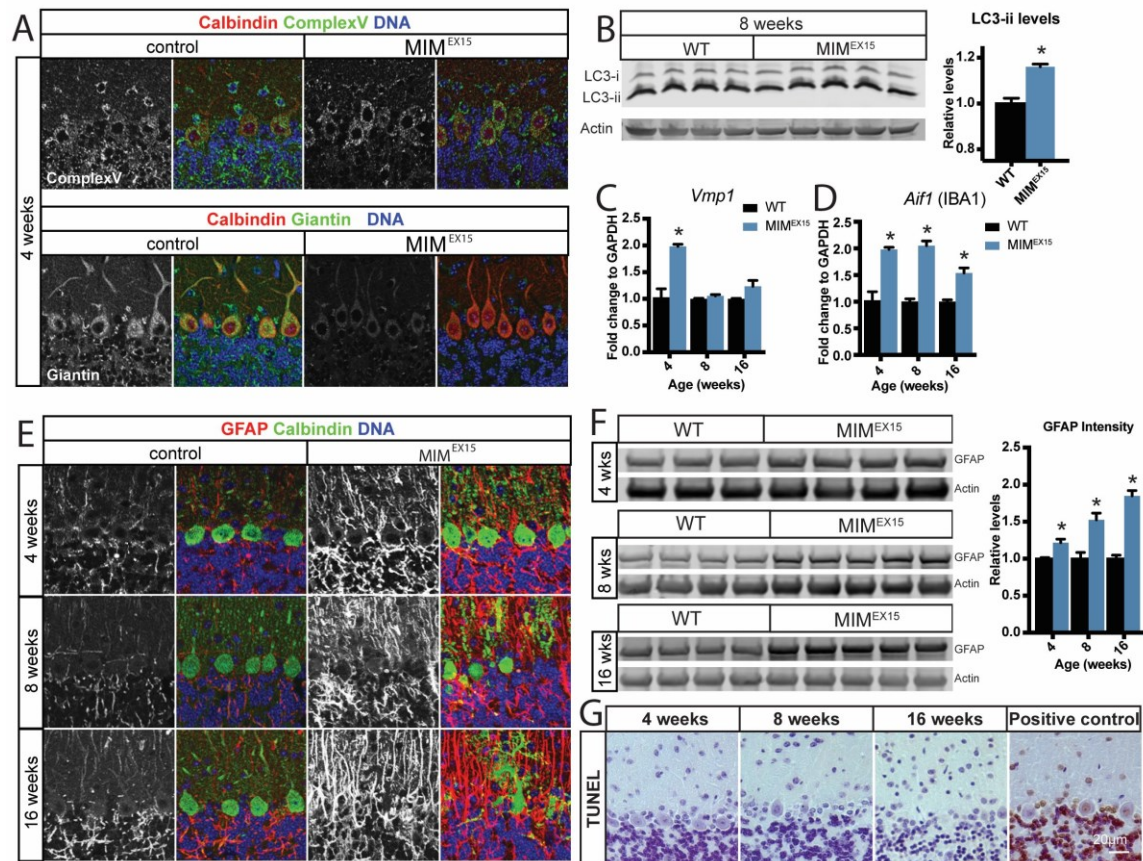


Figure 2



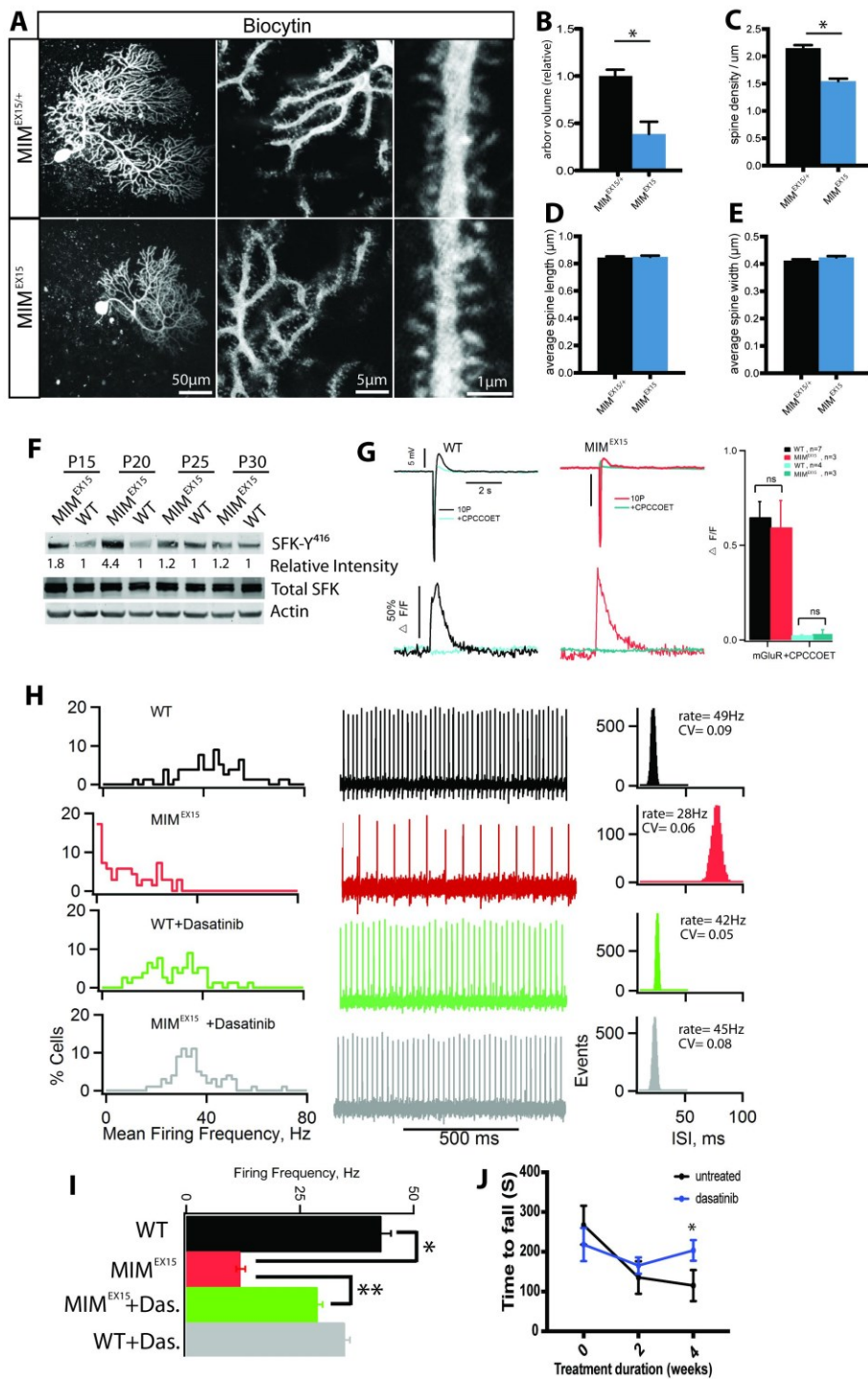


Figure 3

Figure 4

